applied sciences

MDPI

Article

Microdosimetry Study of Proton Quality Factor Using Analytic Model Calculations

Alexis Papadopoulos [1], Ioanna Kyriakou [1,*], Yusuke Matsuya [2,3], Sébastien Incerti [4], Ioannis A. Daglis [5,6] and Dimitris Emfietzoglou [1]

1 Medical Physics Laboratory, Department of Medicine, University of Ioannina, 45110 Ioannina, Greece
2 Nuclear Science and Engineering Center, Research Group for Radiation Transport Analysis, Japan Atomic Energy Agency (JAEA), 2-4 Shirakata, Tokai, Ibaraki 319-1195, Japan
3 Faculty of Health Sciences, Hokkaido University, Kita-12 Nishi-5, Kita-ku, Sapporo 060-0812, Japan
4 CNRS, LP2I Bordeaux, UMR 5797, University of Bordeaux, F-33170 Gradignan, France
5 Department of Physics, National and Kapodistrian University of Athens, 15784 Athens, Greece
6 Hellenic Space Center, 15231 Athens, Greece
* Correspondence: ikyriak@uoi.gr

Abstract: The quality factor (Q) is formally linked to the stochastic (e.g., carcinogenic) risk of diverse ionizing radiations at low doses and/or low dose rates. Q can be a function of the non-stochastic physical quantity Linear Energy Transfer (LET) or the microdosimetric parameter lineal energy (y). These two physical quantities can be calculated either by Monte Carlo (MC) track-structure simulations or by analytic models. In this work, various generalized analytical models were utilized and combined to determine the proton lineal energy spectra in liquid water spheres of various sizes (i.e., 10–3000 nm diameter) over the proton energy range of 1–250 MeV. The calculated spectra were subsequently used within the Theory of Dual Radiation Action (TDRA) and the ICRU Report 40 microdosimetric methodologies to determine the variation of $\overline{Q}$ with proton energy. The results revealed that the LET-based Q values underestimated the microdosimetric-based $\overline{Q}$ values for protons with energy below ~100 MeV. At energies relevant to the Bragg peak region (<20–30 MeV), the differences were larger than 20–50%, while reaching 200–500% at ~5 MeV. It was further shown that the microdosimetric-based $\overline{Q}$ values for protons below ~100 MeV were sensitive to the sphere size. Finally, condensed-phase effects had a very small (<5%) influence on the calculated microdosimetric-based $\overline{Q}$ over the proton energy range considered here.

Keywords: microdosimetry; relative biological effectiveness; quality factor; proton therapy; space radiation; carcinogenic risk

Citation: Papadopoulos, A.; Kyriakou, I.; Matsuya, Y.; Incerti, S.; Daglis, I.A.; Emfietzoglou, D. Microdosimetry Study of Proton Quality Factor Using Analytic Model Calculations. *Appl. Sci.* **2022**, *12*, 8950. https://doi.org/10.3390/app12188950

Academic Editor: Maria Filomena Botelho

Received: 1 August 2022
Accepted: 30 August 2022
Published: 6 September 2022

1. Introduction

As energetic ions interact with matter, they dissipate energy to atoms and molecules in a unique and stochastic manner. To a good approximation, non-relativistic energetic ions interact with the medium mostly by inelastic Coulomb-force collisions with atomic electrons, leading to ionizations and electronic excitations. An important observation is that radiation effects depend upon the spatial pattern of energy deposition which is distinct for each type and energy of radiation. This is termed radiation quality [1–4].

Radiation quality plays a major role in the radiobiological effects observed in living matter, and it is commonly described by relative biological effectiveness (RBE). To a first approximation, RBE is a function of the (unrestricted) Linear Energy Transfer (LET), which is defined as the mean electronic energy-loss by a primary charged particle per unit path length. LET may be conveniently calculated from Bethe's stopping-power theory [5]. The official connection of LET with radiation quality (or RBE) has been made by the International Commission on Radiation Protection (ICRP) in a series of reports [3,4,6]. According to the ICRP, the quality factor, Q, is defined as the low-dose RBE (or RBE_{max})

for stochastic effects [3] and may be expressed as a continuous function of LET [4]. More recently, LET has been used in several empirical RBE models for tissue reactions (or deterministic effects) in the context of hadron therapy [7–11].

Despite its simplicity and wide applicability, there are well-known physical limitations of the LET concept [12], which are more profound when the site of interest is reduced to cellular and subcellular structures (micrometres to nanometres). The most notable limitation of LET is that it neglects the stochastic nature of energy deposition (energy-loss straggling) from the charged particle to the medium while no consideration is given to the finite range of secondary electrons (δ-rays). Although the restricted LET, L_Δ, which excludes those δ-rays with energy above a cut-off value Δ, can be used to better approximate the energy retained in the site, it still refers to a mean value and does not account for straggling [13].

The above limitations of LET can be overcome using microdosimetric approaches [13–15]. For example, classical (or regional) microdosimetry considers a fixed-size critical site in which energy deposition distributions are linked to radiobiological effects. More advanced microdosimetric approaches (e.g., structural microdosimetry [14]) are available with the cost of increased calculation complexity and computing time.

Lineal energy has been widely exploited in radiation quality studies as a measurable physical quantity by tissue-equivalent proportional counters (TEPC), also called Rossi counters [16]. The biophysical justification of connecting lineal energy with RBE (or Q) is provided by the Theory of Dual Radiation Action (TDRA) [17]. The official connection of lineal energy with Q has been made by the International Commission on Radiation Units and Measurements (ICRU) in its Report 40 [2]. The lineal energy has also been used in RBE studies of cell toxicity in the context of hadron therapy through the Microdosimetric-Kinetic Model (MKM) [18–20]. Other microdosimetric-based models of Q used by NASA for space radiation can be found in several published works [21–25]. Q is used to determine the quantity effective dose which corresponds to the stochastic (mainly carcinogenic) risk of irradiated individuals. In turn, the effective dose is used to calculate the number of safe days in space, a vital quantity for manned missions such as those to the Moon and Mars, i.e., the maximum number of days that astronauts can spend in space without exceeding their radiation dose limits. In proton radiotherapy, the effective dose is used to quantify the secondary cancer risk in healthy tissues that are exposed to stray proton radiation.

Measurements of lineal energy are typically limited to simulated tissue volumes larger than tens of nanometres, i.e., they exclude volumes relevant to DNA-sized critical structures [13,15]. Theoretical calculations of lineal energy often employ Monte-Carlo track structure (MCTS) codes, such as GEANT4-DNA [26], KURBUC [27], PARTRAC [28] and PHITS [29], among others [30,31]. Many such efforts for determining the microdosimetric spectra for protons and heavier ions are available in literature [32–45]. MCTS codes simulate, collision-by-collision, all the interactions between the primary (and secondary) particles and the atoms/molecules of the medium (commonly liquid water) until all particles (primaries and secondaries) become non-ionizing (i.e., fall below about 10 eV). Thus, MCTS codes enable simulations with nanometre resolution, including the explicit simulation of radiation-induced DNA damage at various levels of sophistication [46,47]. However, MCTS simulations are well known for being time-intensive while requiring a fair amount of computer expertise.

Analytical models for calculating lineal energy spectra can overcome many of the above difficulties as they are based on simple mathematical expressions that approximate the energy-loss process. Such models have been developed in a series of papers by Xapsos [48–51] and Olko [52,53]. The main idea is to analytically calculate the dependence of lineal energy upon LET while adding suitable correction terms for the effect of energy-loss straggling and the finite range of δ-rays.

The aim of this paper was to: (i) compare and combine various analytical models for calculating the microdosimetric parameter y_D for protons in the energy range of 1–250 MeV for different sphere diameters (10, 100, 1000, 3000 nm); (ii) use the calculated y spectra to determine the variation of the quality factor (Q) with proton energy according to both the

TDRA and ICRU Report 40 microdosimetric methodologies and compare against the LET-based ICRP Report 60 recommendations; (iii) compare the analytical model calculations against published MCTS data of y_D and corresponding $\overline{Q}$; (iv) examine the sensitivity of the results to the choice of target sphere size and water-medium transport parameters (gas vs. liquid).

2. Materials and Methods

2.1. Microdosimetric Calculations of Lineal Energy (y)

In classical microdosimetry, radiation quality is not represented by LET, but rather by its stochastic analogue, the lineal energy, y [1]. Contrary to LET, lineal energy represents the actual energy imparted (ε) in a volume by a single primary particle (along with all its secondary particles) divided by the mean chord length of that volume ($\bar{l}$). The energy imparted to the matter in a volume, ε, is a stochastic quantity that equals the summation of all individual energy transfers (ε_κ) which result from the interactions of the primary charged particle with the atomic electrons:

$$\varepsilon = \sum_k \varepsilon_k \tag{1}$$

The quantity lineal energy, y, is the quotient of ε divided by the mean chord length, $\bar{l}$, of the volume of interest:

$$y = \frac{\varepsilon}{\bar{l}}. \tag{2}$$

For a convex body, $\bar{l} = \frac{4V}{A}$, with A being the area and V its volume [1,13,14]. It follows that for a sphere, $\bar{l} = \frac{2}{3}d$, where d is the sphere's diameter. Lineal energy refers to a single event, that is, one primary particle that randomly traverses the volume of interest. It is important to recognize that, contrary to LET, lineal energy depends not only on radiation quality, i.e., the type and energy of the radiation, but also on the size (and shape) of the target volume (via $\bar{l}$) [13,14]. Furthermore, since y is a stochastic quantity, each radiation quality is represented by a distribution of y values (which is again contrary to LET). Therefore, we may define two mean values of y, namely, its frequency-mean lineal energy defined by [1]:

$$y_F = \int y f(y) \mathrm{d}y \tag{3}$$

with $f(y)$ being the probability density function, and its dose-mean lineal energy defined by:

$$y_D = \frac{1}{y_F} \int y^2 f(y) \mathrm{d}y \tag{4}$$

The physical quantities defined above (y, y_F, y_D) are used in various definitions of Q as discussed in subsequent sections (Section 2.3).

2.2. Generalized Analytic Microdosimetric Models

2.2.1. The Xapsos et al. 1994 Model

In this model (hereafter denoted as "X94"), the energy deposition inside the target volume is classified as either "direct" or "indirect". The former is related to the energy deposition by a primary ion crossing the target, whereas the latter is related to the energy deposition by δ-rays produced by an ion passing outside the target [48]. The contribution of direct (ion) and indirect (δ-rays) energy deposition events varies with the kinetic energy of the ion and the diameter of the target volume. For example, with increasing ion energy and/or volume size, the indirect contribution is enhanced by δ-rays become more energetic and/or have a higher probability to reach the target volume.

To a first approximation, when an ion crosses a volume, the energy deposited is proportional to the product of LET and the mean chord length $\bar{l}$. However, for insufficient (e.g., approaching the nanometer scale), energy loss-straggling, path length fluctuations

and energy carried out of the volume by δ-rays may become pronounced. It can be shown that the y_D can be calculated as a function of distributions of LET, path length and single-collision energy-transfer [48]. The corresponding expressions for the direct (ion, $y_{D,ion}$), indirect (δ-ray, $y_{D,el}$) and total events are [48]:

$$y_{D,ion} = \frac{1}{\bar{l}}(f_{ion} L_{D,ion} s_{D,ion} + \delta_{2,ion}), \tag{5}$$

$$y_{D,el} = \frac{1}{\bar{l}}(L_{D,el} s_{D,el} + \delta_{2,el}), \tag{6}$$

$$y_D = f_{ion} y_{D,ion} + (1 - f_{ion}) y_{D,el}, \tag{7}$$

where f_{ion} is the fraction of energy deposited in the site by the primary ion. The calculation of each parameter (f_{ion}, $\delta_{2,ion}$, $\delta_{2,el}$, $L_{D,ion}$, $L_{D,el}$, $s_{D,ion}$, $s_{D,el}$) entering the above expressions, Equations (5)–(7), is discussed below.

When an ion traverses a site, it deposits energy and generates δ-rays (i.e., secondary electrons) that, subsequently, may deposit only a fraction (or all) of their energy inside the site. The fraction of ion energy that is retained inside the site may be described analytically by the spatially restricted LET. Then, it may be shown that [54,55]:

$$f_{ion} = \frac{\ln[\frac{T_{el,max}(\Delta+\Delta1+\Delta2)}{\bar{l}^2}]}{2\ln[\frac{T_{el,max}}{I}]}, \tag{8}$$

where I is the mean excitation energy of the stopping-power of the medium, and $T_{el,max}$ is the maximum energy that an ion can transfer to a secondary electron (δ-ray):

$$T_{el,max} = 2.179\ T_{ion}, \tag{9}$$

with T_{ion} expressed in (MeV/amu) and $T_{el,max}$ in keV. Δ is the energy of an electron with range equal to the mean chord length of the site, Δ1 accounts for the energy transferred by escaping secondary electrons to the site and Δ2 is the electronic excitation or ionization energy present in the atoms after the interaction with the ion (i.e., binding effects) when secondary electrons migrate outside the volume. It holds that [48,49,54]:

$$(\Delta1 + \Delta2) = \left(1 - \frac{\Delta}{T_{el,max}}\right)(I + \Delta). \tag{10}$$

The dose-weighted mean-energy deposited in the site by ions in a single inelastic collision ($\delta_{2,ion}$) is obtained from:

$$\delta_{2,ion} = \frac{Min[\Delta, T_{el,max}]}{2\ln[\frac{Min[\Delta, T_{el,max}]}{I}]}, Min[\Delta, T_{el,max}] \leq 1\text{keV} \tag{11}$$

$$\delta_{2,ion} = A\Delta^B,\ Min[\Delta, T_{el,max}] \geq 1\text{keV}, \tag{12}$$

with $\delta_{2,ion}$ in units of keV. For protons in water vapor, the values A = 0.190 and B = 0.621 have been suggested [48]. The corresponding expressions for electrons are:

$$\delta_{2,el} = \frac{0.2105\overline{T}_{el}}{\ln\left[\frac{\overline{T}_{el}}{2I}\right] - 0.193},\ \ \overline{T}_{el} \geq 2\text{ keV}, \tag{13}$$

$$\delta_{2,el} = A\overline{T}_{el}{}^B,\ \ \overline{T}_{el} \leq 2\text{ keV} \tag{14}$$

with parameters A = 0.114 and B = 0.591 for water vapor [48]. Note that the condition $Min[\Delta, T_{el,max}]$ for the ion case, Equation (11), is now replaced by $\overline{T}_{el}/2$, which is the maxi-

mum energy transfer in an electron-electron collision. $\overline{T}_{el}$ is the average energy of secondary electrons, which may be represented by the fitted expression [48]:

$$\overline{T}_{el} = 1.25T_{ion}^{0.229}\Delta^{0.778+0.00142\ T_{ion}}, \quad (15)$$

with $\overline{T}_{el}$ and Δ in keV and T_{ion} in MeV/amu.

The dose-averaged LET ($\overline{L}_{D,ion}$ and $\overline{L}_{D,el}$) in Equations (5) and (6) equal the ratio $\overline{L^2}/\overline{L}$. For the case of monoenergetic ions that cross the volume with almost constant LET, the ratio $\overline{L^2}/\overline{L}$ reduces to LET, i.e., $\overline{L}_{D,ion}$ = LET$_{ion}$. For electrons, the dose-averaged LET can differ significantly for different volumes and energies. It can be shown that [48]:

$$\overline{L}_{D,el} = \begin{cases} 0.985\ \text{LET}_{el}(\Delta + 0.02), & \Delta \le I \\ 0.925\text{LET}_{el}(\Delta + 0.05), & \Delta \ge I \end{cases}. \quad (16)$$

Finally, the path length moment ratio ($\overline{s}_{D,ion}$, $\overline{s}_{D,el}$) for a sphere is equal to $3d/4$ for both ion and electron [14,48,49].

Equations (8)–(16) can then be implemented into Equations (5) and (6) to calculate y_D from Equation (7).

2.2.2. The Xapsos et al. 1996 Model

This model (hereafter denoted as "X96") treats only direct events but uses an explicit description of ion's energy-loss straggling. Specifically, the probability density function, $p_{x,s}$, for energy deposition x along an ion's path length s (for a single traversal), is approximated by a log-normal distribution:

$$p_{x,s} = \frac{1}{\sqrt{2\pi}\sigma_s x} Exp[-\left(\frac{(\ln(x) - \mu_s)}{\sqrt{2}\sigma_s}\right)^2], \quad (17)$$

where μ_s and σ_s are the mean and variance of the distribution, respectively. They can be calculated from:

$$\mu_s = \ln(\overline{x}_{ion}) - 0.5\sigma_s^2, \quad (18)$$

$$\sigma_s = \sqrt{\ln(1+V)}, \quad (19)$$

where $\overline{x}_{ion}$ is the mean energy deposited in the site for s equal to the mean chord length of the site, and V is obtained as a sum of various contributing terms:

$$V = V_{str} + V_s + V_L + V_F + V_L V_s. \quad (20)$$

The terms in Equation (20) are as follows: $V_{str} = \frac{\delta_{2,ion}}{\overline{\varepsilon}_{ion}}$ is the relative variance of energy-loss straggling [48,55], where $\delta_{2,ion}$ is taken from Equations (11) and (12). $\overline{\varepsilon}_{ion} = f_{ion}$ LET$_{ion}s$ is the mean energy deposited in the target volume as a function of ion's path length (s), V_s is the relative variance of ion's path length distribution, V_L is the relative variance of ion's LET distribution and V_F is the relative variance of Fano fluctuations. For monoenergetic ions and neglecting the Fano fluctuations, Equation (20) reduces to [48,49]:

$$V = V_{str} + V_s. \quad (21)$$

The Fano fluctuations are needed in studies of ionization fluctuations. Here, we studied the energy deposition, so it was not necessary to include it in Equation (21) [48,49]. Then, the total probability density function, f_x for energy deposition x, is the convolution of the straggling distribution $p_{x,s}$ and the probability density function of the particle's path length inside the site, c_s.

$$f_x = \int p_{x,s} c_s \mathrm{d}s. \quad (22)$$

For a sphere, and assuming that ions travel in straight lines [48,49], $c_s = 2s/d^2$.

2.2.3. The Combined Xapsos Models

The extension of the X96 model to the indirect (electron) events may be developed following the X94 model (the combined model is hereafter denoted as "Xcom"). The relative variance of electron events may be calculated from Equation (21),with the addition of a term related to the relative variance of LET (V_L), with $V_{str} = \delta_{2,el}/\bar{\varepsilon}_{el}$, where $\delta_{2,el}$ is obtained from Equations (13) and (14) and $\bar{\varepsilon}_{el} = \overline{\mathrm{LET}}_{el}s$, where $\overline{\mathrm{LET}}_{el}$ is the mean slowed-down electron LET [48,50]. Then, the combined probability density for energy distribution is given by:

$$f_x = Pf_{x,ion} + (1-P)f_{x,el}, \tag{23}$$

where P is the fraction of direct events. The fraction of indirect events $(1-P)$ is given by [50]:

$$(1-P) = \frac{(1-f_{ion})\bar{x}_{ion}}{f_{ion}\bar{x}_{el} + (1-f_{ion})\bar{x}_{ion}}, \tag{24}$$

where $\bar{x}_{el}$ is the mean energy deposited in the site, in an analogous interpretation as $\bar{x}_{ion}$.

2.2.4. The Combined Xapsos-Olko Model

In this model [52] (hereafter denoted as "XO"), Xcom is used for the calculation of energy deposition and the microdosimetric spectra of the ion (direct) and electron (indirect) events. Specifically, to calculate the ion (direct events) energy deposition, one uses the Equations (8)–(12) and (17)–(24) from the 'X96' model. For the electron energy deposition (indirect events), one uses Equations (13) and (14) and Equations (17)–(24) for energy-loss straggling, relative variance, and the log-normal process of energy deposition, respectively. However, contrary to the Xcom model, in the XO model one uses the full secondary electron spectrum which is calculated using the following expressions [52]:

$$\bar{L}_{el} = \frac{\int_{3W}^{T_{el,max}} L_{el}(K)\varphi(K)\mathrm{d}K}{\int_{3W}^{T_{emax}} \varphi(K)\mathrm{d}K}, \tag{25}$$

where W is the energy required for an ion-electron hole. $\varphi(K)$ is the degraded electron spectra given by:

$$\varphi(T) = \frac{\int_{T}^{T_{el,max}} T'^{-2}\mathrm{d}T'}{L_{el}(T)}. \tag{26}$$

To visualise the central assumptions of the present microdosimetric models, Figure 1 depicts the two ways in which the energy can be deposited (direct, indirect) on a spherical site of arbitrary diameter.

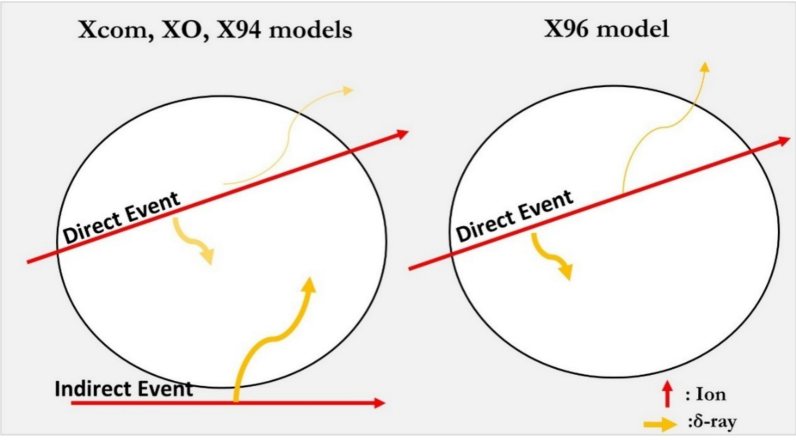

Figure 1. Schematic representation of the energy deposition on an arbitrary spherical target from ions (direct events) and δ-rays (indirect events), used by the present analytical models (Xcom, XO, X94, X96).

2.3. Methods for Calculating the Quality Factor (Q)

2.3.1. The TDRA Approach

According to the site model of the Theory of Dual Radiation Action (TDRA), the RBE for a high-LET radiation can be obtained from the following expression [13]:

$$RBE_{TDRA} = \frac{\sqrt{z_{D,L}{}^2 + 4D_H(z_{D,H} + D_H)} - z_{D,L}}{2D_H}, \quad (27)$$

where $z_{D,H}$ and $z_{D,L}$ are the dose-average specific energy of the high- and low-LET radiation, respectively, and D_H is the absorbed dose of the high-LET radiation. For the low-dose range of interest in the present study (recall that $Q = RBE_{D\to 0}$), we may assume that $D_H \ll z_{D,L}$ and Equation (27) reduce to the expression ($z_D = ky_D$), with k being a normalisation constant) [56]:

$$\overline{Q_{TDRA}} = \frac{y_{D,test}}{y_{D,ref}}, \quad (28)$$

where $y_{D,test}$ and $y_{D,ref}$ are the y_D for the radiation under test and the reference radiation, respectively.

2.3.2. The ICRU Report 40 Recommendation

The International Commission on Radiation Units and Measurements (ICRU) Report 40 was the first to officially link the quality factor Q with the microdosimetric quantity lineal energy (y) using the following analytic expression:

$$Q_{ICRU40} = \frac{5510}{y}\left[1 - Exp\left(-5 \times 10^{-5}y^2 - 2 \times 10^{-7}y^3\right)\right]. \quad (29)$$

As a result, for a specific proton energy, the mean quality factor $\overline{Q}$ can be calculated from:

$$\overline{Q} = \frac{\int Q_{ICRU40}(y_{test})d(y_{test})dy}{\int Q_{ICRU40}(y_{ref})d(y_{ref})dy}, \quad (30)$$

where $d(y)$ is the dose-weighted distribution of lineal energy defined by $d(y) = (y/y_F)f(y)$. The difficulties in understanding the effects of high-LET radiation, and thus in the calculation of $\overline{Q}$, were compensated by the choice of a quantity that can be measured and at the same time be physically appropriate. Therefore, lineal energy was to be determined in a tissue-equivalent sphere with a diameter equal to 1 µm, which is experimentally feasible using TEPCs.

2.3.3. The ICRP Report 60 Recommendation

For radiation protection purposes, the International Committee on Radiation Protection (ICRP) Report 60, expressed the quality factor (Q) as a function of LET in water, $Q(L)$. The particular mathematical expression of $Q(L)$ was deduced on the basis of various in vitro and animal radiobiological studies [3]. The recommended LET dependence of Q is as follows:

$$Q(L) = 1, \; L < 10 \text{ keV}/\mu\text{m} \quad (31)$$

$$Q(L) = 0.32L - 2.2\,, \;\; 10\text{keV}/\mu\text{m} \leq L \leq 100 \text{ keV}/\mu\text{m} \quad (32)$$

$$Q(L) = \frac{300}{\sqrt{L}}, \; L > 100 \text{ keV}/\mu\text{m} \quad (33)$$

2.4. Modifications of Model Parameters

To calculate the microdosimetric parameter y_D using the above models (X94, Xcom, XO), we must first establish the needed material parameters, namely the mean excitation energy of stopping-power theory (I) (entering Equations (8), (10) and (11)), the constants A and B (of Equations (12) and (14)) and the cut-off energy Δ. The choice of the cut off

energy Δ is defined by the electron energy that corresponds to a penetration depth equal to the mean chord length $\bar{l} = \frac{2d}{3}$ of the target size. For reasons of availability, the original implementation of X94 and X96 models used data for condensed water vapor. Vapor water refers to the so-called gas phase approximation, whereby interaction cross sections for water vapor are extrapolated to unit density medium. Therefore, vapor and liquid water share the same density (and also both temperature and pressure values) but differ upon the underlying physics of their interaction cross sections. Specifically, vapor water cross sections do not account for intermolecular effects (screening, etc.) which are considered (according to the theoretical model adopted) in the case of liquid water. To examine the degree of which the results are sensitive to the parameters of the water medium, we here deduced the corresponding parameters for liquid water. Table 1 summarizes the values of the model parameters used in the present work. The cut-off energy Δ for the different sphere diameters was estimated from electron penetration-depth values for liquid water obtained from Geant4-DNA MC simulations using the latest electron physics list (Option 4) for liquid water [57]. The corresponding values for condensed water vapour were determined from the analytic fitting formulas for the electron penetration-depth obtained by the MC4 code [58]. For the calculation of the material constants, A and B, for electrons and protons, we followed the method described in Xapsos et al. (1994), whereby Equations (11) and (12) and their derivatives, with respect to $Min[\Delta, T_{el,max}] = \Delta$, are continuous at a Δ value that equals twice the K-shell binding energy of water (2 × 540 eV = 1.08 keV).

Table 1. Physical model parameters used in the present work for liquid and vapor water (both at unit density).

Physical Parameters	Liquid Water	Vapor Water	Reference
I value (keV)	0.078	0.071	Liquid: ICRU Report 90 [5] Vapor: ICRU Report16 [59]
Δ-cut off electron energy (keV)	11.0 (d = 3 μm) 5.62 (d = 1 μm) 1.37 (d = 0.1 μm) 0.184 (d = 0.01 μm)	11.1 (d = 3 μm) 5.93 (d = 1 μm) 1.50 (d = 0.1 μm) 0.288 (d = 0.01 μm)	Liquid: Kyriakou et al. (2016) [57] Vapor: Emfietzoglou et al. (2008) [58]
δ2-energy-weighted mean energy deposited inside the target per collision (keV)	Protons: A = 0.195, B = 0.610 Electrons: A = 0.121, B = 0.577	Protons: A = 0.190, B = 0.620 Electrons: A = 0.114, B = 0.591	Liquid: Our fit Vapor: Xapsos et al. (1994) [48]

3. Results

The quality factor (Q) is a relative parameter that quantifies the risk of stochastic effects (e.g., carcinogenesis) of different ionizing radiations in comparison to a predefined "reference" radiation. For convenience, we used the proton energy of 100 MeV here as the reference radiation (i.e., the quality factor of 100 MeV proton was set to unity). This choice is convenient for the direct comparison of $\overline{Q}$ calculated by analytic models and Monte-Carlo data, since the latter data used in this work are only available up to 100 MeV. None of the conclusions of the work would have changed if another proton energy was chosen.

3.1. Dose-Averaged Lineal Energy and Quality Factor

Figure 2 presents y_D values for a liquid water sphere of 1 μm diameter over the proton energy range of 1–250 MeV. Proton beams with initial energy between 50 and 250 MeV are increasingly used in cancer radiotherapy. For space applications, protons in the Van Allen belts reach up to 400 MeV. After these protons interact with spacecraft shielding, they slow down. Those capable of penetrating within the spacecraft reach the astronauts with energies well below 300 MeV. Moreover, protons in the energy range below 30 MeV make up the Bragg peak region where the $\overline{Q}$ (and the carcinogenic risk) becomes maximum. The calculated values are from the different analytical models examined in the present work (X94, Xcom, XO), as well as published MC data by Geant4-DNA [60] and TEPC simulations

by the PITS99-KURBUC [46] codes. For better visualisation, the y_D values in the energy range of 1–100 MeV are also presented logarithmically in the inset of Figure 2. Note that the available Geant4-DNA and TEPC simulation data are limited up to 100 MeV.

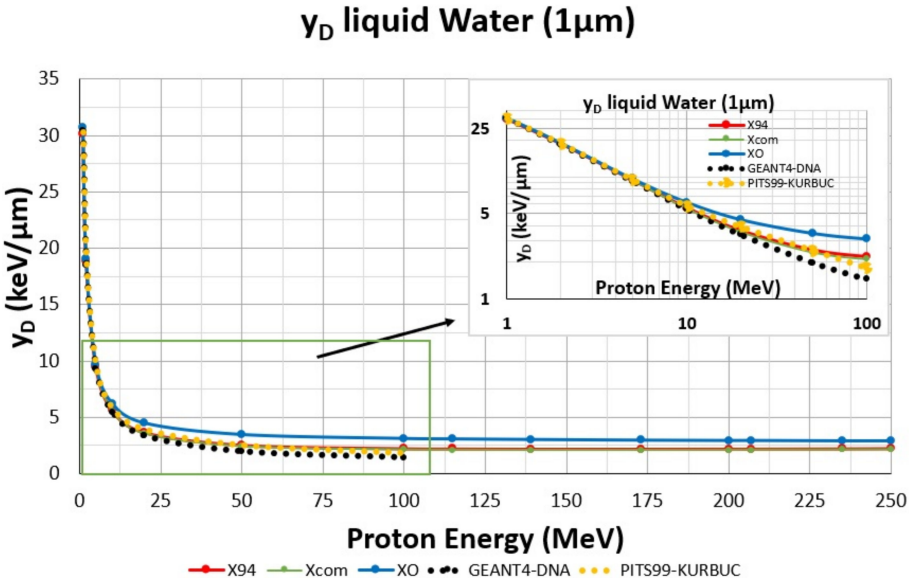

Figure 2. y_D values for a liquid water sphere of 1 µm diameter as a function of proton energy calculated by the different analytic models examined (X94, Xcom, XO), and Monte Carlo data by the Geant4-DNA code [60] and TEPC simulations with PITS99-KURBUC [46]. Inset: Logarithmical presentation of the y_D values for the energy range of 1–100 MeV.

3.2. Sensitivity of Results to Target Size

Subsequently, the y_D values depicted in Figure 2 along with the full microdosimetric spectra $f(y)$ and $d(y)$ were used to determine the corresponding proton $\overline{Q}$ based on the TDRA and ICRU Report 40 expressions Equations (28) and (30), respectively. Figure 3 presents the calculated $\overline{Q}$ values for the different analytic models (X94, XO, Xcom) and MC data from the Geant4-DNA and TEPC simulation. The LET-based Q values recommended by ICRP Report 60 are also presented for comparison. Figure 4 presents the differences of the microdosimetric-based $\overline{Q}$ values (TDRA, ICRU Report 40) against the LET-based ICRP Report 60 recommendations.

Figure 5 presents y_D values for liquid water spheres of different diameters (10, 100, 1000 nm). The calculated values were from the Xcom analytical model (combination of Xapsos et al. 1994 and Xapsos et al. 1996 models) and the MC data for the different spheres were taken from Geant4-DNA [60]. The Xcom model represents the best available analytic model for calculations of y spectra (please see Appendix A for the fitted values of y_D and the $\overline{Q}_{TDRA}$ of the Xcom model). It combines both the energy deposition and its fluctuations from ion (direct) and electron (indirect) events in the target site, as well as the effects of the finite range of δ-rays. A form of this model has been utilised for determining y spectra in TEPC measurements [50,51]. Similar to Figure 2, the available Geant4-DNA data for these spheres are limited up to 100 MeV.

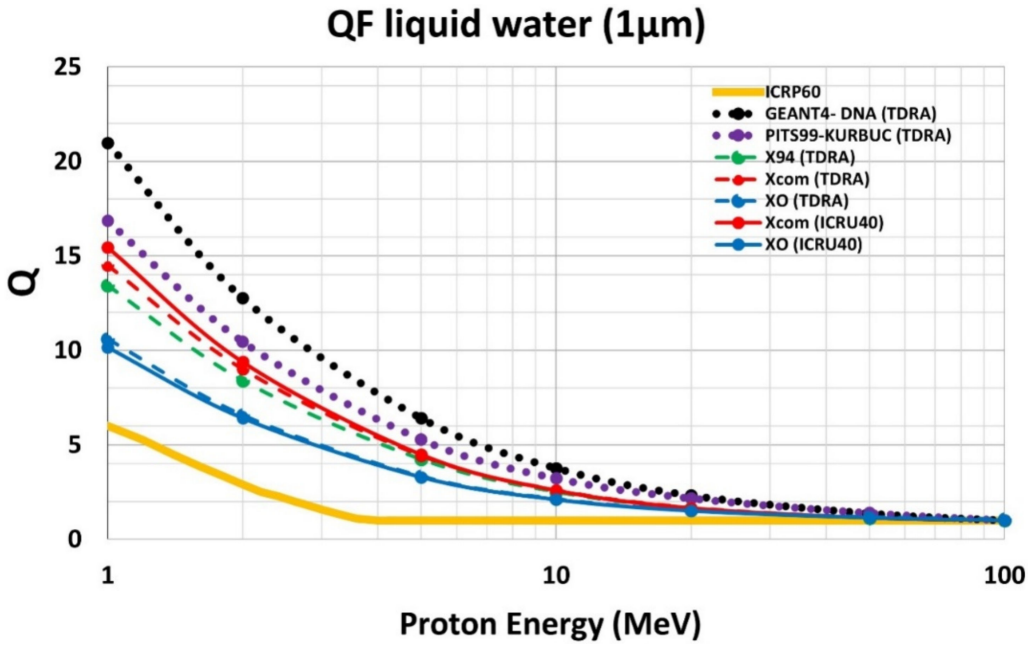

Figure 3. Energy variation of the proton $\overline{Q}$ based on different microdosimetric approaches (TDRA, ICRU Report 40) with input data from both analytic models (X94, XO, Xcom) and Monte-Carlo codes (Geant4-DNA [60], TEPC simulations by PITS99-KURBUC [46]). The microdosimetric data pertain to a liquid water sphere of 1 µm diameter. The LET-based Q values recommended by ICRP Report 60 are also shown for comparison.

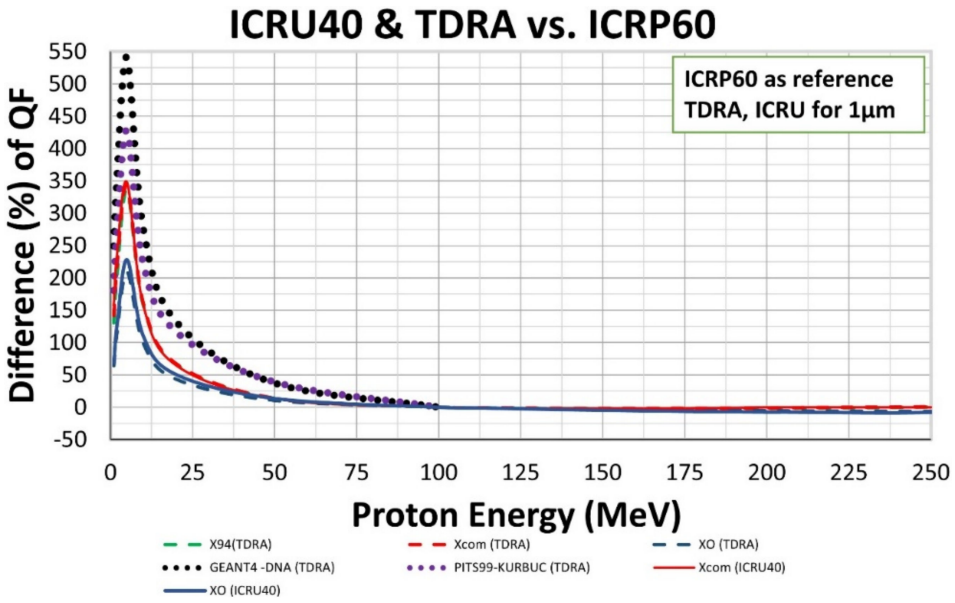

Figure 4. Difference (%) of TDRA and ICRU Report 40 predictions for the proton $\overline{Q}$ with input data calculated by different analytic models (X94, XO, Xcom) and Monte-Carlo codes (Geant4DNA [60], TEPC simulations by PITS99-KURBUC [46]). All microdosimetric calculations pertain to a liquid water sphere of 1 µm diameter. The LETbased Q values recommended by ICRP Report 60 were used as baseline for comparison.

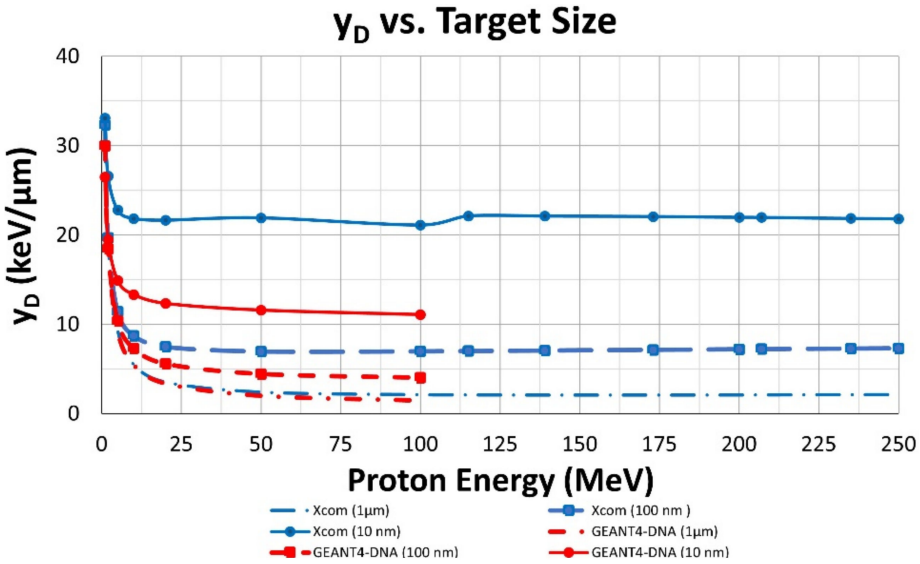

Figure 5. y_D values as a function of proton energy for liquid water spherical volumes of 10, 100 and 1000 nm diameter calculated by the Xcom analytic model (blue lines) and the MonteCarlo data of Geant4-DNA [56] (red lines).

Using the y_D values of Figure 5, Figure 6 presents the corresponding $\overline{Q}$ for sphere diameters of 100 nm and 10 nm using the TDRA approach, Equation (28), over the proton energy range of 1–100 MeV. The LET-based Q values from the ICRP60 recommendations are also shown for comparison. In Figure 7, the differences (%) of the TDRA-based $\overline{Q}$ for 100 nm and 10 nm calculated by the Xcom analytic model and the Geant4-DNA MC data are presented with the LET-based Q values of ICRP Report 60 recommendations used as baseline.

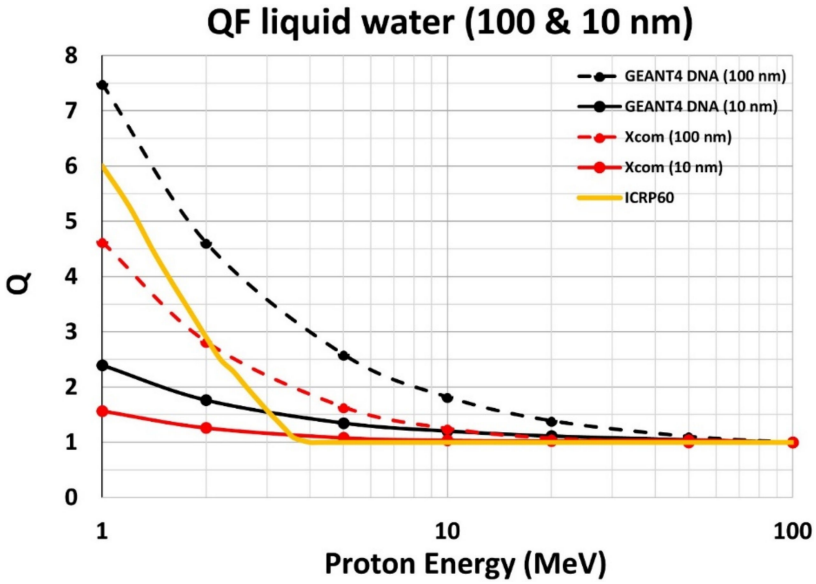

Figure 6. Energy variation of the proton $\overline{Q}$ based on the TDRA approach with input data from the Xcom analytic model (red colour) and the Geant4DNA Monte-Carlo code [60] (black colour). The microdosimetric data pertain to a liquid water spheres of 0.1 and 0.01 µm diameter. The LETbased Q values recommended by ICRP Report 60 are also shown for comparison (dark yellow colour).

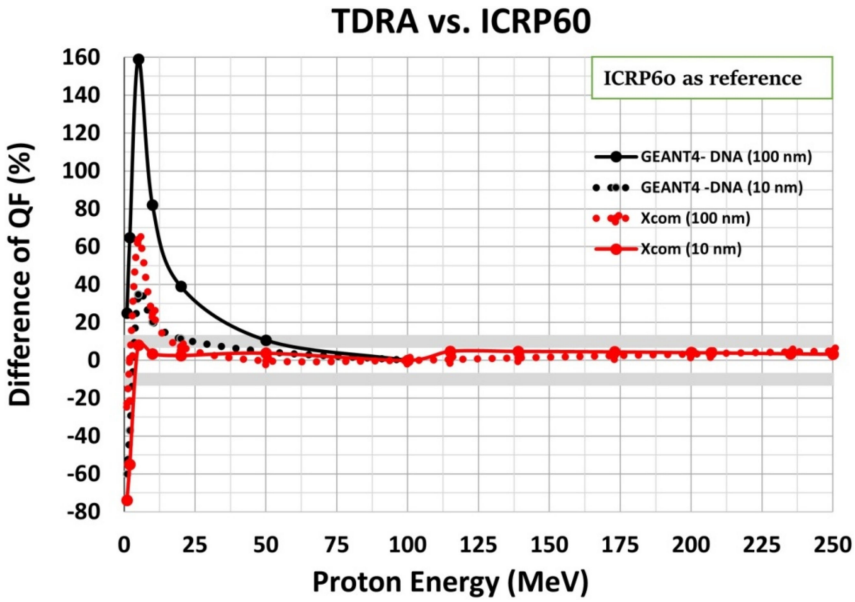

Figure 7. Difference (%) of the TDRA-based $\overline{Q}$ calculated by the Xcom analytic model and the Geant4-DNA Monte-Carlo data [60] for 0.1 and 0.01 μm liquid water spheres. The LET-based Q values recommended by ICRP Report 60 were used as baseline for comparison.

Based on the results of Figures 5 and 6, the sensitivity of proton $\overline{Q}$ with respect to sphere diameter is depicted in Figure 8 with the $\overline{Q}$ value at 1 μm diameter used as baseline for the comparison.

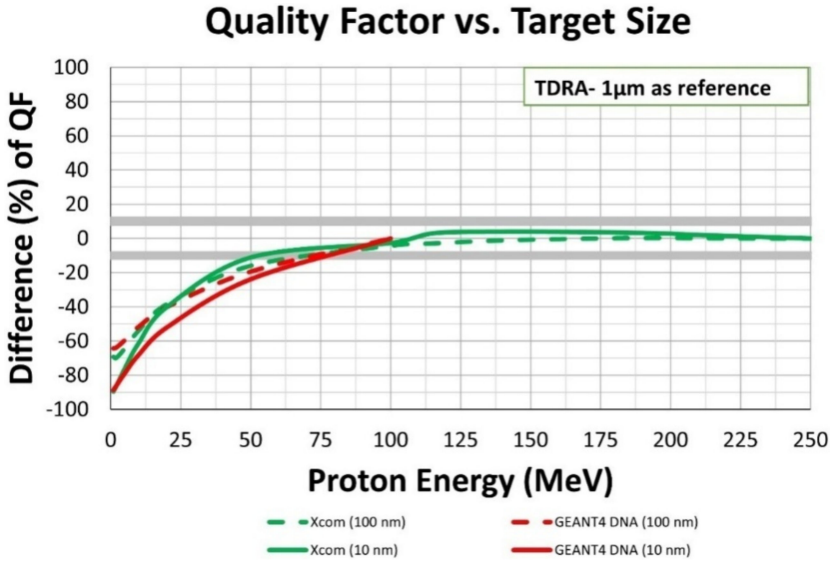

Figure 8. Difference (%) of TDRAbased proton $\overline{Q}$ calculated by the Xcom analytic model (green colour) and the Geant4DNA Monte-Carlo data [60] (red colour). The corresponding results for 1 μm were used as baseline for comparison.

3.3. Sensitivity of Results to Condensed-Phase Effects

Figures 9 and 10 show the differences of y_D and corresponding $\overline{Q}$, respectively, between gaseous and liquid water (both at unit density) based on the examined analytic models (X94, Xcom and XO) with input parameters according to Table 1. Results are shown for spherical volumes with 3000, 1000, 100 and 10 nm diameter and for proton energies from 1 to 250 MeV. At each sphere size, the results of liquid water were used as baseline for the comparison.

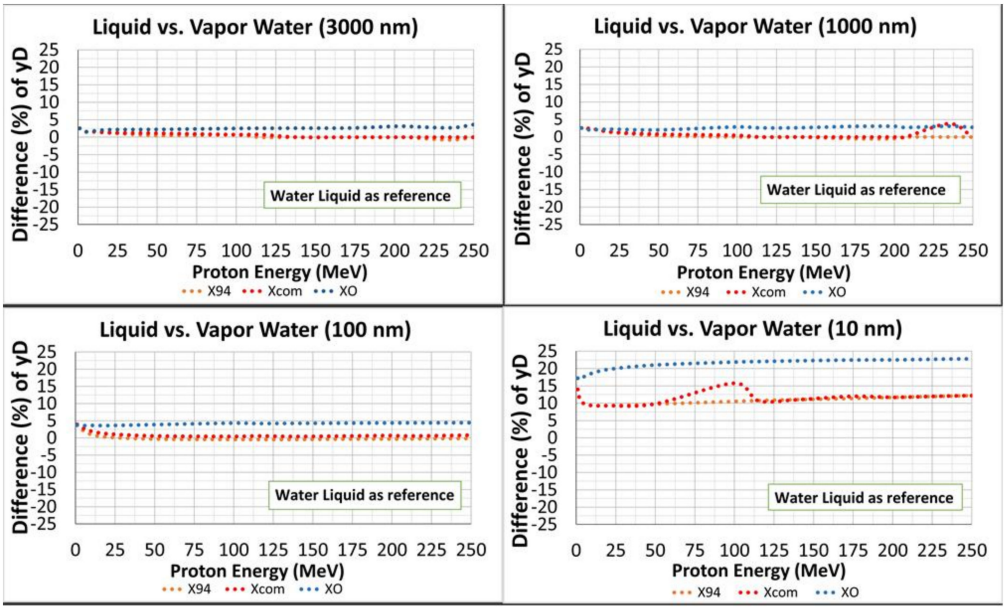

Figure 9. Difference (%) of y_D for unit-density gaseous and liquid water spherical volumes of different diameter (10, 100, 1000, 3000 nm) calculated by the different analytic models. The liquid water values were used as baseline for comparison.

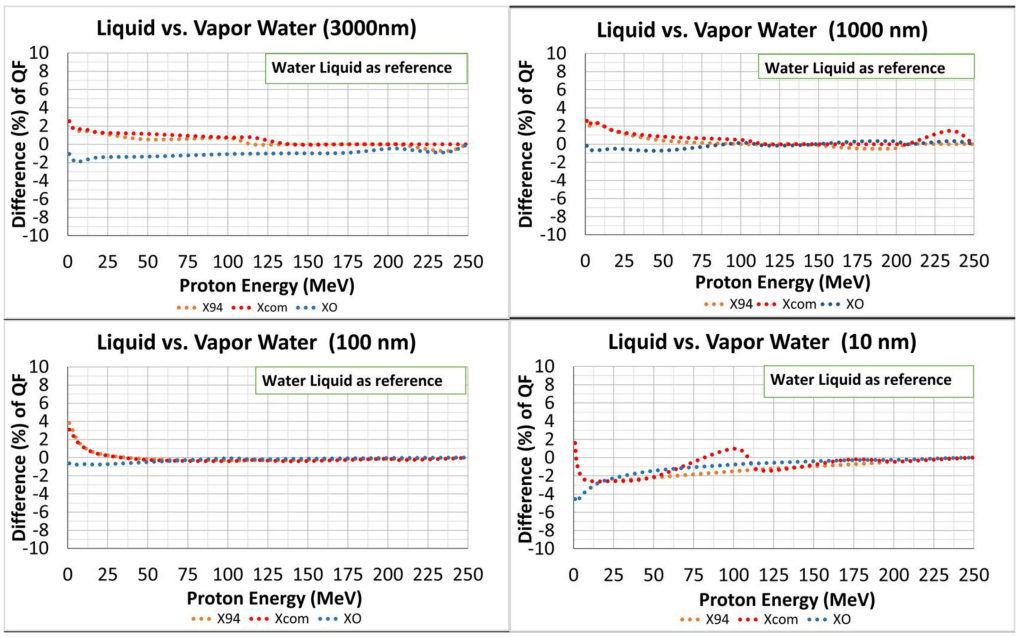

Figure 10. Difference (%) of TDRA-based proton $\overline{Q}$ between unit density gaseous and liquid water spheres of varying diameter calculated by the different analytic models. The liquid water values were used as baseline for comparison.

4. Discussion

As it can be seen from Figure 2 the calculated y_D values for 1μm target size and for proton energies 1–250 MeV calculated by the different analytical models (X94, Xcom, XO) followed the same trend over the whole energy range. The difference between the X94 and Xcom models reached up to 10% while the XO model was consistently higher by up to 40–50% in the energy range of 50–250 MeV. This is due to the different calculation of the deposited energy of secondary electrons that affects both the indirect (electron) events and the δ-ray escape from the volume. The secondary electron spectrum is treated differently in the XO and Xcom models; specifically, in the XO model, the full slowing-down spectrum

is used. For the 1 μm sphere, and combining Equations (16) and (24), the mean LET of the secondary electrons calculated by the XO model inside the sphere target is larger than the mean LET calculated by the Xcom model. Higher LET means more energy deposited inside the sphere, so there was a slight increase in the total y_D value for the XO model. The proton energy deposition is treated similarly in both models. Unfortunately, there are no updated references for these discrepancies among the models except the one already cited in out text [48–52]. To our knowledge, the present work represents the first time that all models were combined and compared with $\overline{Q}$ calculations. Importantly, the MC literature data (Geant4-DNA, PITS99-KURBUC) on proton lineal energy has followed similar trends with the analytic calculations. Specifically, the differences between the analytical models (X94 and Xcom) and the MC data (Geant4-DNA, PITS99-KURBUC) did not exceed 10% up to 50 MeV, increasing up to 15–30% in the energy range of 50–100 MeV. The magnitude of this difference is comparable to the difference among the MC data (i.e., Geant4-DNA vs. PITS99-KURBUC), which is up to 10% for proton energies 1–50 MeV and up to 25% for the 50–100 MeV range. Extensive information about the physical models and assumptions made in the MC simulations by Geant4-DNA and PITS99-KURBUC codes can be found in the literature [46,60].

The comparison of the microdosimetric-based proton $\overline{Q}$ values (using TDRA and ICRU Report 40 methodologies, both at 1 μm sphere) against the LET-based ICRP Report 60 recommendations showed noticeable differences (>10–20%) below about 50–75 MeV, reaching a factor of 2–3 at ~5 MeV (see Figures 2 and 3). It is noteworthy that these differences increased further when MC literature data from Geant4-DNA and TEPC simulations from PITS99-KURBUC were used to calculate $\overline{Q}$ by the TDRA. In particular, at energies relevant to the Bragg peak region (<20–30 MeV), the deviations of both the analytic and MC microdosimetric-based $\overline{Q}$ values from ICRP Report 60 agreed above 20–50%.

It follows from Figure 5 that, as the sphere diameter decreased to 100 and 10 nm, the differences in the y_D values between the analytical model calculations and the Geant4-DNA MC data became more pronounced at lower energies (~5–10 MeV). This is expected given that at smaller volumes, the details of how the energy-loss processes (including the effect of straggling and δ-ray production and transport) are considered in each approach (analytical models vs. MC simulations) become more important for the energy imparted to the site. The present models (Xcom, X94, XO) are generally recommended for diameters greater than several nanometers, specifically for diameters much larger than the penetration range of electrons with energy equal to the mean excitation energy of the medium (I) which, in this case, translates to d > 2 nm. In general, for space applications, diameters in the range of 1000–3000 nm are most relevant to experimental TEPC measurements (e.g., ISS). In addition, several studies of proton (and carbon) RBE in hadron therapy have suggested that y_D should be determined in spheres with 10–15 nm diameter [15]. The present work reveals that the results of analytic models (and MC simulations) already diverge below 100 nm. Therefore, even larger discrepancies are expected for spheres with d < 10 nm. The influence of sphere size on the TDRA $\overline{Q}$ values seem to be significant (>10%) only below ~50 MeV (see Figures 6–8). The y_D values of high-energy protons were found to be sensitive to the choice of the sphere size due to the contribution of the energetic secondary electrons (δ-rays). Specifically, for high-energy protons, there are more indirect events (Equation (24)), and the mean LET of these electrons is often equal to or even larger than that of the high-energy proton, resulting in a strong increase in y_D. Therefore, when calculating the TDRA quality factor for the low-energy protons, by normalizing to a reference radiation (Equation (28))—which, in this study, is a high-energy proton (100 MeV)—it results in a large variation of $\overline{Q}$. Calculations of the $\overline{Q}$ based on ICRU Report 40 have also been performed for nanometer targets (10–100 nm). However, only the values for 1 μm are shown since Equation (29) is deduced for this particular sphere size. It is somewhat surprising that with decreasing sphere size (from 1 μm to 100 and 10 nm), the $\overline{Q}$ values by TDRA are in better agreement with the ICRP Report 60 recommendations than the $\overline{Q}$ values by TDRA based on the conventional 1 μm sphere. On the other hand, larger

sphere diameters (>1 μm) were found to yield even higher deviations from ICRP Report 60 (not presented).

The present work is, to our knowledge, the first study that systematically combines and compares the most established analytical microdosimetric models for proton $\overline{Q}$ calculations. Proton quality factors are continuously used by various space organizations and the radiotherapy community to assess the carcinogenic risk of irradiated individuals, e.g., for long-duration manned missions and/or in the context of the organs at risks (OAR) in proton therapy, respectively. Although LET-based calculations of Q are generally preferred in practical applications due to the availability of LET values for various ions over a wide energy range, it is recognized that microdosimetric-based calculations offer a scientifically sounder approach (ICRU 40). However, the difficulties of working with microdosimetric quantities, which are stochastic in nature, has led to a situation where experimental microdosimetric measurements with TEPC are often approximated by some average LET values before their practical implementation. The combination of available analytic models discussed in the present work further supports the use of microdosimetric-based approaches to proton quality factor problems as a viable alternative to LET-based approaches. An important finding of the present study is the energy range over which LET-based and y-based proton $\overline{Q}$ values may differ substantially. Specifically, the low-energy range (1–50 MeV) corresponds to protons that comprise the Bragg peak region, where the absorbed dose becomes maximum and variation of $\overline{Q}$ are expected to have a major impact in absolute terms. It is also relevant to protons that penetrate a typical astronaut spacesuit (>10 MeV) during an Extra Vehicular Activity (EVA) or those generated (as secondary radiation) inside the astronaut's body during a deep space mission. It should be noted that both the European Space Agency (ESA) and the Canadian Space Agency (CSA) presently adopt the LET-based ICRP Report 60 recommendations for $\overline{Q}$.

A common concern in microdosimetric calculations at sub-micron volumes is the influence of the condensed phase, i.e., the difference of microdosimetric spectra between gaseous and liquid water (at the same density). The results of Figures 9 and 10 clearly show that, although such effects may influence the analytical model calculations of y_D by up to 20% for the smallest sphere examined (10 nm diameter), the end effect on $\overline{Q}$ is negligible (<5%).

5. Conclusions

Different analytical microdosimetric models have been used and combined for calculating the microdosimetric quantity y_D for target spheres of various sizes. The lineal energy spectra were subsequently used to study the variation of the proton $\overline{Q}$ over the energy range of 1–250 MeV based on the TDRA and ICRU Report 40 microdosimetric methodologies. The microdosimetric-based $\overline{Q}$ values reveal that the LET-based ICRP Report 60 recommendations may significantly underestimate $\overline{Q}$ for proton energies below ~50–100 MeV. Similar trends were found when MC track-structure literature data were used as input to the calculations. The microdosimetric-based $\overline{Q}$ values for low-energy protons were also found to be sensitive to the choice of the sphere size. Finally, condensed-phase effects in the analytic model parameters had only a weak influence on $\overline{Q}$ in the examined range of proton energies and sphere sizes. Although the general trend of the variation of $\overline{Q}$ with proton energy revealed by the present analytic model calculations is supported by the MC literature data used in this work, future research will include a systematic comparison and validation of lineal energy spectra and subsequent calculations of $\overline{Q}$ based on new MC data with the latest versions of Geant4-DNA and PHITS track structure codes which make use of different and updated physics models.

Author Contributions: Conceptualization, D.E., I.K., Y.M., S.I. and I.A.D.; methodology, A.P. and D.E.; software, A.P. and Y.M.; validation, I.K. and Y.M.; formal analysis, A.P.; investigation, A.P.; data curation, Y.M.; writing—original draft preparation, A.P.; writing—review and editing, D.E., I.K., Y.M., S.I. and I.A.D.; supervision, D.E., I.K., S.I. and I.A.D.; project administration, I.K. and I.A.D.;

funding acquisition, D.E., I.K. and S.I. All authors have read and agreed to the published version of the manuscript.

Funding: This research was funded by the project "Dioni: Computing Infrastructure for Big-Data Processing and Analysis". (MIS No. 5047222) which is implemented under the Action "Reinforcement of the Research and Innovation Infrastructure", funded by the Operational Programme "Competitiveness, Entrepreneurship and Innovation" (NSRF 2014–2020) and co-financed by Greece and the European Union (European Regional Development Fund), as well as by the European Space Agency (ESA) under contract "BioRad III" 4000132935/21/NL/CRS (2021–2023).

Institutional Review Board Statement: Not applicable.

Data Availability Statement: Not applicable.

Conflicts of Interest: The authors declare no conflict of interest.

Appendix A

To facilitate the use of the microdosimetric parameter y_D and the calculation of Q, we fitted the corresponding values of the Xcom model for the proton energy range of 1–100 MeV and for 1000, 100 and 10 nm spheres of liquid water. The Xcom model was chosen due to the availability of the input data in the literature, as well as the fact that it seems to be the most complete and validated generalized analytical model. The proton range 1–100 MeV was chosen because most validated data from MCTS simulations reach up to this energy. The general trend of the y_D and Q values can be represented by a fitted function of the form

$$f(T) = (c + \frac{a}{T^b})^d, \quad \text{(A1)}$$

where the coefficients a, b, c and d have different values for each sphere diameter (see Table A1). The differences (%) between the fitted values $y_{D,fitted}$ based on Equation (A1) and the y_D values calculated by the Xcom model are shown in Figure A1. The fitted values were mostly within 10% for all sphere diameters and proton energies.

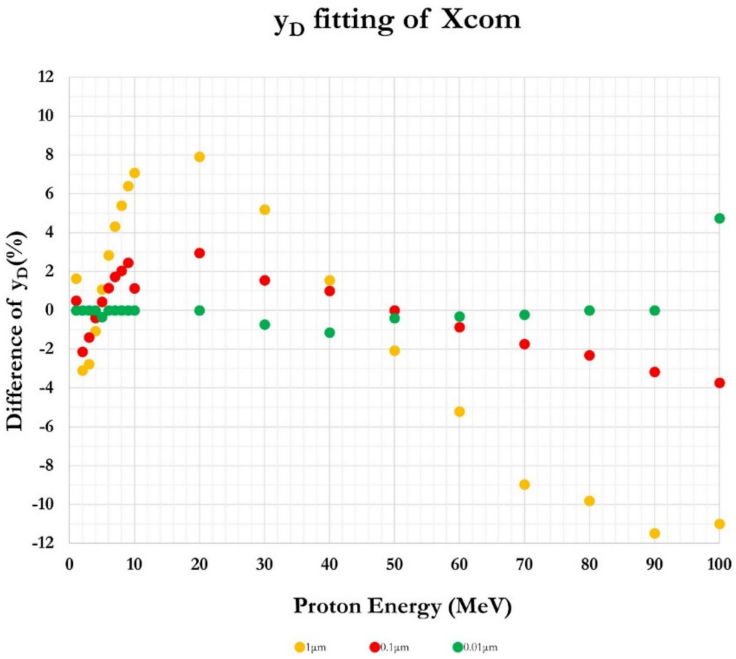

Figure A1. Differences (%) of y_D values calculated from the fitting Equation (A1) and the Xcom model. The values of the Xcom model were used as baseline for comparison.

The differences between the fitted Q_{fitted} values based on Equation (A1) and the calculated Q values from the Xcom model are shown in Figure A2. The fitted values were mostly within 10% for all sphere diameters and proton energies.

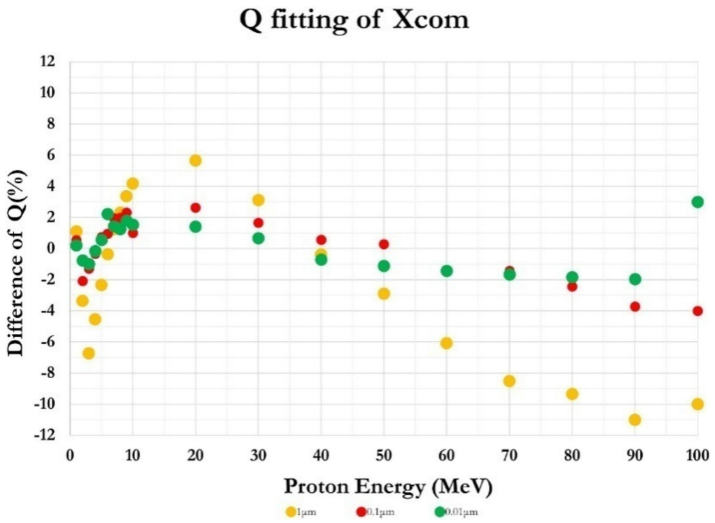

Figure A2. Differences (%) of quality factor (Q) values calculated from the fitting Equation (A1) and the Xcom model. The values of the Xcom model were used as baseline for comparison.

Table A1. Values of the constants a, b, c and d which are needed for the calculation of dose-mean lineal energy (y_D) and the quality factor (Q) using Equation (A1).

Diameter (d) in µm	Parameters	*a*	*b*	*c*	*d*
1	$y_{D,fitted}$	30.24	0.788	0.97	1
	Q_{fitted}	36.20	1	0.514	0.744
0.1	$y_{D,fitted}$	25.89	1.024	6.470	1
	Q_{fitted}	3.723	1.025	0.930	1
0.01	$y_{D,fitted}$	11.46	1.349	21.77	1
	Q_{fitted}	0.540	1.380	1.030	1

References

1. International Commission on Radiation Units and Measurements (Ed.) *Microdosimetry*; ICRU Report; International Commission on Radiation Units and Measurements: Bethesda, MD, USA, 1983; ISBN 978-0-913394-30-4.
2. Joint Task Group on Radiation Protection Quantities; International Commission on Radiological Protection; International Commission on Radiation Units and Measurements (Eds.) *The Quality Factor in Radiation Protection: Report of a Joint Task Group of the ICRP and the ICRU to the ICRP and the ICRU*; ICRU Report; International Commission on Radiation Units and Measurements: Bethesda, MD, USA, 1986; ISBN 978-0-913394-34-2.
3. International Commission on Radiological Protection. *1990 Recommendations of the International Commission on Radiological Protection*, 1st ed.; ICRP Publication Radiation Protection; Pergamon Press: Oxford, UK, 1991; ISBN 978-0-08-041144-6.
4. ICRP. *Recommendations of the ICRP*; ICRP Publication 26; Pergamon Press: Oxford, UK, 1977.
5. International Commission on Radiation Units and Measurements. Journal of the ICRU 2014, 14, NP.1-NP. Available online: https://journals.sagepub.com/description/cru (accessed on 20 August 2022).
6. ICRP. *Recommendations of the International Commission on Radiological Protection*; ICRP Publication 9; Pergamon Press: Oxford, UK, 1966.
7. Wilkens, J.J.; Oelfke, U. A Phenomenological Model for the Relative Biological Effectiveness in Therapeutic Proton Beams. *Phys. Med. Biol.* **2004**, *49*, 2811–2825. [CrossRef] [PubMed]
8. Carabe, A.; Moteabbed, M.; Depauw, N.; Schuemann, J.; Paganetti, H. Range Uncertainty in Proton Therapy Due to Variable Biological Effectiveness. *Phys. Med. Biol.* **2012**, *57*, 1159–1172. [CrossRef] [PubMed]
9. Wedenberg, M.; Lind, B.K.; Hårdemark, B. A Model for the Relative Biological Effectiveness of Protons: The Tissue Specific Parameter α/β of Photons Is a Predictor for the Sensitivity to LET Changes. *Acta Oncol.* **2013**, *52*, 580–588. [CrossRef] [PubMed]
10. McNamara, A.L.; Schuemann, J.; Paganetti, H. A Phenomenological Relative Biological Effectiveness (RBE) Model for Proton Therapy Based on All Published in Vitro Cell Survival Data. *Phys. Med. Biol.* **2015**, *60*, 8399–8416. [CrossRef]
11. Paganetti, H.; Blakely, E.; Carabe-Fernandez, A.; Carlson, D.J.; Das, I.J.; Dong, L.; Grosshans, D.; Held, K.D.; Mohan, R.; Moiseenko, V.; et al. Report of the AAPM TG-256 on the Relative Biological Effectiveness of Proton Beams in Radiation Therapy. *Med. Phys.* **2019**, *46*, e53–e78. [CrossRef]
12. Kellerer, A.M.; Chmelevsky, D. Criteria for the Applicability of LET. *Radiat. Res.* **1975**, *63*, 226. [CrossRef]

13. Rossi, H.H.; Zaider, M. *Microdosimetry and Its Applications*; Springer: Berlin/Heidelberg, Germany, 2012; ISBN 978-3-642-85184-1.
14. Kellerer, A.M. *Fundamentals of Microdosimetry*; Universitätsbibliothek der Ludwig-Maximilians-Universität München: München, Germany, 1985.
15. Lindborg, L.; Lillhök, J.; Kyriakou, I.; Emfietzoglou, D. Dose-mean lineal energy values for electrons by different Monte Carlo codes: Consequences for estimates of radiation quality in photon beams. *Med. Phys.* **2022**, *49*, 1286–1296. [CrossRef]
16. Rossi, H.H.; Rosenzweig, W. A Device for the Measurement of Dose as a Function of Specific Ionization. *Radiology* **1955**, *64*, 404–411. [CrossRef]
17. Kellerer, A.M.; Rossi, H.H. A Generalized Formulation of Dual Radiation Action. *Radiat. Res.* **1978**, *75*, 471. [CrossRef]
18. Hawkins, R.B. A Statistical Theory of Cell Killing by Radiation of Varying Linear Energy Transfer. *Radiat. Res.* **1994**, *140*, 366. [CrossRef]
19. Hawkins, R.B. A Microdosimetric-Kinetic Theory of the Dependence of the RBE for Cell Death on LET. *Med. Phys.* **1998**, *25*, 1157–1170. [CrossRef]
20. Hawkins, R.B. A Microdosimetric-Kinetic Model of Cell Death from Exposure to Ionizing Radiation of Any LET, with Experimental and Clinical Applications. *Int. J. Radiat. Biol.* **1996**, *69*, 739–755. [CrossRef]
21. Cucinotta, F.A.; To, K.; Cacao, E. Predictions of Space Radiation Fatality Risk for Exploration Missions. *Life Sci. Space Res.* **2017**, *13*, 1–11. [CrossRef]
22. Cucinotta, F.A.; Cacao, E.; Alp, M. Space Radiation Quality Factors and the Delta Ray Dose and Dose-Rate Reduction Effectiveness Factor. *Health Phys.* **2016**, *110*, 262–266. [CrossRef]
23. Cucinotta, F.A.; Kim, M.Y.; Chappell, L. *Space Radiation Cancer Risk Projections and Uncertainties*; NASA: Washington, DC, USA, 2013; p. 207375.
24. Cucinotta, F.A. A New Approach to Reduce Uncertainties in Space Radiation Cancer Risk Predictions. *PLoS ONE* **2015**, *10*, e0120717. [CrossRef]
25. Borak, T.B.; Heilbronn, L.H.; Townsend, L.W.; McBeth, R.A.; de Wet, W. Quality Factors for Space Radiation: A New Approach. *Life Sci. Space Res.* **2014**, *1*, 96–102. [CrossRef]
26. Incerti, S.; Baldacchino, G.; Bernal, M.; Capra, R.; Champion, C.; Francis, Z.; Guèye, P.; Mantero, A.; Mascialino, B.; Moretto, P.; et al. The GEANT4-DNA Project. *Int. J. Model. Simul. Sci. Comput.* **2010**, *1*, 157–178. [CrossRef]
27. Uehara, S.; Nikjoo, H.; Goodhead, D.T. Cross-Sections for Water Vapour for the Monte Carlo Electron Track Structure Code from 10 EV to the MeV Region. *Phys. Med. Biol.* **1993**, *38*, 1841–1858. [CrossRef]
28. Kundrát, P.; Friedland, W.; Becker, J.; Eidemüller, M.; Ottolenghi, A.; Baiocco, G. Analytical Formulas Representing Track-Structure Simulations on DNA Damage Induced by Protons and Light Ions at Radiotherapy-Relevant Energies. *Sci. Rep.* **2020**, *10*, 15775. [CrossRef]
29. Sato, T.; Iwamoto, Y.; Hashimoto, S.; Ogawa, T.; Furuta, T.; Abe, S.; Kai, T.; Tsai, P.-E.; Matsuda, N.; Iwase, H.; et al. Features of Particle and Heavy Ion Transport Code System (PHITS) Version 3.02. *J. Nucl. Sci. Technol.* **2018**, *55*, 684–690. [CrossRef]
30. Dingfelder, M. Track-Structure Simulations for Charged Particles. *Health Phys.* **2012**, *103*, 590–595. [CrossRef]
31. Nikjoo, H.; O'Neill, P.; Terrissol, M.; Goodhead, D.T. Modelling of Radiation-Induced DNA Damage: The Early Physical and Chemical Event. *Int. J. Radiat. Biol.* **1994**, *66*, 453–457. [CrossRef] [PubMed]
32. Perales, Á.; Baratto-Roldán, A.; Kimstrand, P.; Cortés-Giraldo, M.A.; Carabe, A. Parameterising Microdosimetric Distributions of Mono-Energetic Proton Beams for Fast Estimates of y_D and y*. *Biomed. Phys. Eng. Express* **2019**, *5*, 045014. [CrossRef]
33. Burigo, L.; Pshenichnov, I.; Mishustin, I.; Bleicher, M. Microdosimetry Spectra and RBE of 1H, 4He, 7Li and 12C Nuclei in Water Studied with Geant4. *Nucl. Instrum. Methods Phys. Res. Sect. B Beam Interact. Mater. At.* **2014**, *320*, 89–99. [CrossRef]
34. Newpower, M.; Patel, D.; Bronk, L.; Guan, F.; Chaudhary, P.; McMahon, S.J.; Prise, K.M.; Schettino, G.; Grosshans, D.R.; Mohan, R. Using the Proton Energy Spectrum and Microdosimetry to Model Proton Relative Biological Effectiveness. *Int. J. Radiat. Oncol. Biol. Phys.* **2019**, *104*, 316–324. [CrossRef] [PubMed]
35. Mokari, M.; Moeini, H.; Soleimani, M. Calculation of Microdosimetric Spectra for Protons Using Geant4-DNA and a μ-Randomness Sampling Algorithm for the Nanometric Structures. *Int. J. Radiat. Biol.* **2021**, *97*, 208–218. [CrossRef] [PubMed]
36. Liamsuwan, T.; Hultqvist, M.; Lindborg, L.; Uehara, S.; Nikjoo, H. Microdosimetry of Proton and Carbon Ions: Microdosimetry of P and C Beams. *Med. Phys.* **2014**, *41*, 081721. [CrossRef]
37. Nikjoo, H.; Uehara, S.; Emfietzoglou, D.; Pinsky, L. A Database of Frequency Distributions of Energy Depositions in Small-Size Targets by Electrons and Ions. *Radiat. Prot. Dosim.* **2011**, *143*, 145–151. [CrossRef]
38. Leuthold, G.; Burger, G. Mathematical Simulation of Proton Tracks in Water Vapor and Their Microdosimetric Analysis. *Radiat. Environ. Biophys.* **1988**, *27*, 177–187. [CrossRef]
39. Lindborg, L.; Hultqvist, M.; Carlsson Tedgren, Å.; Nikjoo, H. Lineal Energy and Radiation Quality in Radiation Therapy: Model Calculations and Comparison with Experiment. *Phys. Med. Biol.* **2013**, *58*, 3089–3105. [CrossRef]
40. Liamsuwan, T.; Uehara, S.; Emfietzoglou, D.; Nikjoo, H. Physical and Biophysical Properties of Proton Tracks of Energies 1 KeV to 300 MeV in Water. *Int. J. Radiat. Biol.* **2011**, *87*, 141–160. [CrossRef]
41. Palajová, Z.; Spurný, F.; Davídková, M. Microdosimetry Distributions for 40–200 MeV Protons. *Radiat. Prot. Dosim.* **2006**, *121*, 376–381. [CrossRef]

42. Francis, Z.; El Bitar, Z.; Incerti, S.; Bernal, M.A.; Karamitros, M.; Tran, H.N. Calculation of Lineal Energies for Water and DNA Bases Using the Rudd Model Cross Sections Integrated within the Geant4-DNA Processes. *J. Appl. Phys.* **2017**, *122*, 014701. [CrossRef]
43. Chmelevsky, D.; Kellerer, A.M. Computation of Microdosimetric Distributions for Small Sites. *Radiat. Environ. Biophys.* **1977**, *14*, 123–136. [CrossRef]
44. Chen, J. Microdosimetric Characteristics of Proton Beams from 50 KeV to 200 MeV. *Radiat. Prot. Dosim.* **2011**, *143*, 436–439. [CrossRef]
45. Berger, M.J. Energy Loss Straggling of Protons in Water Vapour. *Radiat. Prot. Dosim.* **1985**, *13*, 87–90. [CrossRef]
46. Nikjoo, H.; Emfietzoglou, D.; Liamsuwan, T.; Taleei, R.; Liljequist, D.; Uehara, S. Radiation Track, DNA Damage and Response—A Review. *Rep. Prog. Phys.* **2016**, *79*, 116601. [CrossRef]
47. Matsuya, Y.; Kai, T.; Sato, T.; Ogawa, T.; Hirata, Y.; Yoshii, Y.; Parisi, A.; Liamsuwan, T. Track-Structure Modes in Particle and Heavy Ion Transport Code System (PHITS): Application to Radiobiological Research. *Int. J. Radiat. Biol.* **2022**, *98*, 148–157. [CrossRef]
48. Xapsos, M.A.; Burke, E.A.; Shapiro, P.; Summers, G.P. Energy Deposition and Ionization Fluctuations Induced by Ions in Small Sites: An Analytical Approach. *Radiat. Res.* **1994**, *137*, 152. [CrossRef]
49. Xapsos, M.A.; Burke, E.A.; Shapiro, P.; Summers, G.P. Probability Distributions of Energy Deposition and Ionization in Sub-Micrometer Sites of Condensed Media. *Radiat. Meas.* **1996**, *26*, 1–9. [CrossRef]
50. Badavi, F.F.; Xapsos, M.A.; Wilson, J.W. An Analytical Model for the Prediction of a Micro-Dosimeter Response Function. *Adv. Space Res.* **2009**, *44*, 190–201. [CrossRef]
51. Shinn, J.L.; Badhwar, G.D.; Xapsos, M.A.; Cucinotta, F.A.; Wilson, J.W. An Analysis of Energy Deposition in a Tissue Equivalent Proportional Counter Onboard the Space Shuttle. *Radiat. Meas.* **1999**, *30*, 19–28. [CrossRef]
52. Czopyk, L.; Olko, P. An Analytical Model for Calculating Microdosimetric Distributions from Heavy Ions in Nanometer Site Targets. *Radiat. Prot. Dosim.* **2006**, *122*, 36–40. [CrossRef] [PubMed]
53. Olko, P.; Booz, J. Energy Deposition by Protons and Alpha Particles in Spherical Sites of Nanometer to Micrometer Diameter. *Radiat. Environ. Biophys.* **1990**, *29*, 1–17. [CrossRef]
54. Xapsos, M.A. A Spatially Restricted Linear Energy Transfer Equation. *Radiat. Res.* **1992**, *132*, 282. [CrossRef]
55. Xapsos, M.A. Applicability of LET to Single Events in Microelectronic Structures. *IEEE Trans. Nucl. Sci.* **1992**, *39*, 1613–1621. [CrossRef]
56. Kyriakou, I.; Tremi, I.; Georgakilas, A.G.; Emfietzoglou, D. Microdosimetric Investigation of the Radiation Quality of Low-Medium Energy Electrons Using Geant4-DNA. *Appl. Radiat. Isot.* **2021**, *172*, 109654. [CrossRef]
57. Kyriakou, I.; Šefl, M.; Nourry, V.; Incerti, S. The Impact of New Geant4-DNA Cross Section Models on Electron Track Structure Simulations in Liquid Water. *J. Appl. Phys.* **2016**, *119*, 194902. [CrossRef]
58. Emfietzoglou, D.; Kostarelos, K.; Hadjidoukas, P.; Bousis, C.; Fotopoulos, A.; Pathak, A.; Nikjoo, H. Subcellular S-Factors for Low-Energy Electrons: A Comparison of Monte Carlo Simulations and Continuous-Slowing-down Calculations. *Int. J. Radiat. Biol.* **2008**, *84*, 1034–1044. [CrossRef]
59. International Commission on Radiation Units and Measurements (Ed.) *Linear Energy Transfer*; ICRU Report; International Commission on Radiation Units and Measurements: Bethesda, MD, USA, 1970.
60. Vassiliev, O.N.; Peterson, C.B.; Cao, W.; Grosshans, D.R.; Mohan, R. Systematic Microdosimetric Data for Protons of Therapeutic Energies Calculated with Geant4-DNA. *Phys. Med. Biol.* **2019**, *64*, 215018. [CrossRef]